Multibound soliton formation in an erbium-doped ring laser with a highly nonlinear resonator

Dmitriy A. Dvoretskiy, Stanislav G. Sazonkin, Igor S. Kudelin, Ilya O. Orekhov, Alexey B. Pnev, Valeriy E. Karasik, Lev K. Denisov

***Abstract*— We have studied the generation of low-noise ultrashort multibound solitons in the telecommunication spectral window in an erbium-doped all-fiber ring laser with a highly-nonlinear resonator mode-locked by a nonlinear polarization evolution effect. The multibound soliton generation is obtained with more than 20 bound dechirped pulses with a duration of ~ 240 fs at a repetition rate of ~ 11.3 MHz (with a signal-to-noise ratio of ~ 73.3 dB), the relative intensity noise is <-140 dBc/Hz, and the Allan deviation of the repetition frequency does not exceed ~$1.3 \cdot 10^{-8}$ with a time averaging window of ~ 100 s.**

***Index Terms*—fiber lasers, fiber nonlinear optics, laser mode locking, ultrafast lasers**

I. Introduction

ULTRA-SHORT pulsed (USP) mode-locked (ML) fiber lasers can be considered as an ideal platform to expand future applications due to the complex nonlinear dynamics with a presence of a high value of a group velocity dispersion (GVD) and a third-order dispersion (TOD) in the laser resonator [1]. The multibound solitons (MBSs) generation regime [2], soliton molecules [1] and soliton crystals [3] involve a bound state a bound state of multiple optical pulses that propagate with a fixed temporal separation through optical fibers. MBSs are of considerable interest in various fields, such as telecommunication transmission systems [1], optical metrology for astronomical spectrograph calibration [4], nonlinear photonic signal processing [5], medical applications [6] and coherent pulse staking amplification [7]. Note that most of the mentioned applications require the long-term and low-noise operation of an MBS laser.

Since the first numerical demonstration in Ref. [8] MBS generation has been experimentally obtained by different ML techniques. For example, the highest repetition rate of up to 10 GHz in fiber lasers can be achieved by active mode locking [9] or even up to 50 GHz in the case of a Kerr comb in a thermally controlled on-chip silica glass microresonator [10]. Passive mode-locking techniques include the generation of an MBS by different kinds of real saturable absorbers such as SESAM [11], carbon nanotubes [1], graphene [12], MoS_2 and Sb_2Te_3 saturable absorbers [13, 14]. MBS generation has also been widely observed in classic NPE-based fiber lasers [15, 16]. Due to the soliton energy quantization effect theoretically investigated in [17] which leads to multiple pulsing it is possible to generate of several hundred solitons in one packet by pump power scaling, as demonstrated in Ref. [18, 19]. Moreover, harmonic mode locking in a Mach–Zehnder fiber laser enables the tunable generation of multiple pulses at a high-repetition-rate [20, 21].

Unfortunately, there are no significant data on the low-noise and reliable long-term performance of the obtained MBS lasers. In this paper, together with [22], we suggest a simple method to achieve the reliable long-term operation of multiple pulses by increasing the nonlinearity of an all-fiber resonator, which leads to the formation of low-noise ultrashort multibound solitons with N ~ 26 bound pulses in an NPE-based ML fiber ring laser.

II. Experimental Setup

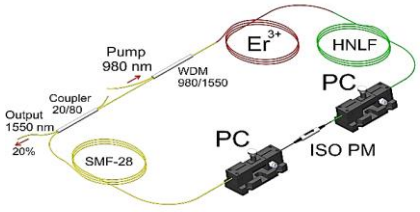

Fig. 1. Experimental setup of the ML EDF ring laser.

The experimental setup of the ML erbium-doped fiber (EDF) ring laser with a highly-nonlinear resonator is shown in Fig. 1. A commercially developed isolator-polarizer (ISO PM) was used as a USP filter for mode locking based on the nonlinear polarization evolution effect and ensured unidirectional generation.

The authors would like to thank A.A. Krylov, S.V. Firstov, A. K. Senatorov, M.A. Likhachev (FORC RAS) for the provision of the active fiber and HNLF, GVD measurements, and a fruitful discussion. The reported study was funded by RFBR, according to the research projects Nos 18-32-20017 and 18-38-00615.

Dmitriy A. Dvoretskiy, Stanislav G. Sazonkin, Ilya O. Orekhov, Alexey B. Pnev, Valeriy E. Karasik, Lev K. Denisov are with Bauman Moscow State Technical University, Moscow 107005 Russia (e-mail: ddvoretskiy@bmstu.ru).

Igor S. Kudelin is with the Aston Institute of Photonics Technologies, Aston University, Aston triangle, Birmingham, B4 7ET, UK (e-mail: kudelini@aston.ac.uk).

This article has been accepted for publication in a future issue of this journal, but has not been fully edited. Content may change prior to final publication. Citation information: DOI 10.1109/LPT.2019.2956570, IEEE Photonics Technology Letters

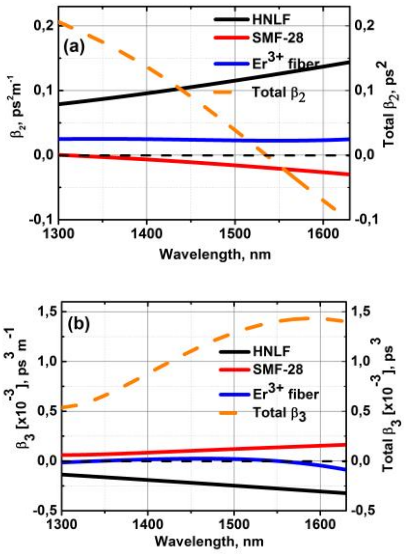

Fig. 2. (a) GVD and β_2 net-cavity dispersion parameter. (b) TOD and β_3 net-cavity dispersion parameter for the ML EDF ring laser.

To adjust the ML regime two polarization controllers (PCs) located at both ends of the ISO PM were included in the ring cavity. We used a pigtailed single mode laser diode operating at 980 nm with a maximum output power of 500 mW as the pump source for the erbium-doped fiber (EDF). An 80/20 fiber coupler was used to lead the laser radiation out of the cavity. The all-fiber ring cavity was formed by a 3.6 m active EDF with a low signal core absorption of ~ 6.5 dB/m at the pump wavelength and a dispersion of D ~ - 17.4 ps/(nm·km) at 1550 nm and a highly nonlinear germanosilicate fiber with a ~50 mol.% concentration of germanium oxide in the core with a dispersion of D ~ - 100 ps/(nm·km) at 1550 nm, ~ 11.5 m SMF-28 fiber (Corning Corp.) with a dispersion of D ~ 17.4 ps/(nm·km) at 1550 nm was used to reduce the total net-cavity GVD into a slightly negative region. The HNLF production parameters were the same as those in [23] and the measured core diameter was ~2.5 μm. The calculated value of the nonlinear refractive index n_2 was $3.63 \cdot 10^{-16}$ cm^2/W. The dispersion parameters β_2 and for the fibers are shown in Fig. 2. The net-cavity dispersion parameters are presented for the HNLF length of L_{HNLF} ~ 1.53 m. Note, that the dispersion parameters β_2 and β_3 have been recalculated from the chromatic dispersion of the fibers measured by the interferometric technique described in [24].

III. Experimental Results and Discussion

Previously we achieved stretched pulse generation in a similar laser resonator with compensated net-cavity GVD and significant third-order dispersion in the highly nonlinear laser resonator [25]. Here we demonstrate multibound soliton formation occurred at the high value of a pump power of ~ 300 mW. The output power versus the pump power is shown in Fig. 3 with a maximum output average power of 30 mW. The MBS ML threshold is observed by means of adjusting both PCs at an average pump power of ~ 300 mW. It should also be pointed out that the control of the PC adjustment at the threshold pump power affected the temporal separation of the ultrashort pulses in the autocorrelation trace and output pulse spectra but did not affect the maximal number of pulses in the bound state. Detailed information about the soliton number evolution in a bunch versus the pump power can be found in our previous paper [26]. Moreover, we did not observe any pulse breaking by increasing the pump power up to 500 mW. The decay of the MBS regime was observed at a pump power of ~ 130 mW. The

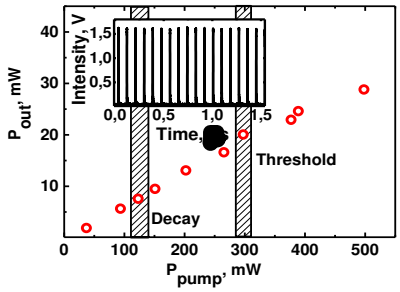

Fig. 3. Pump vs. Output Power. Inset: output pulse trace.

presence of significant hysteresis between the threshold and the decay pump power indicates the generation regime stability, as shown in Ref. [17]. The inset of Fig. 3 shows a typical output pulse trace for the USP generation (using the oscilloscope Infinium MSO9254A; Keysight Technologies, Santa Rosa, CA, USA).

Fig. 4 (a) shows the output multibound soliton generation spectrum in arbitrary units and on a dB scale (inset) with the spectral dependence of the net-cavity GVD. It should be noted that the MBS generation regime occurred only in the slightly negative region close to zero of the net-cavity GVD and with the presence of an uncompensated TOD (see Fig. 2).

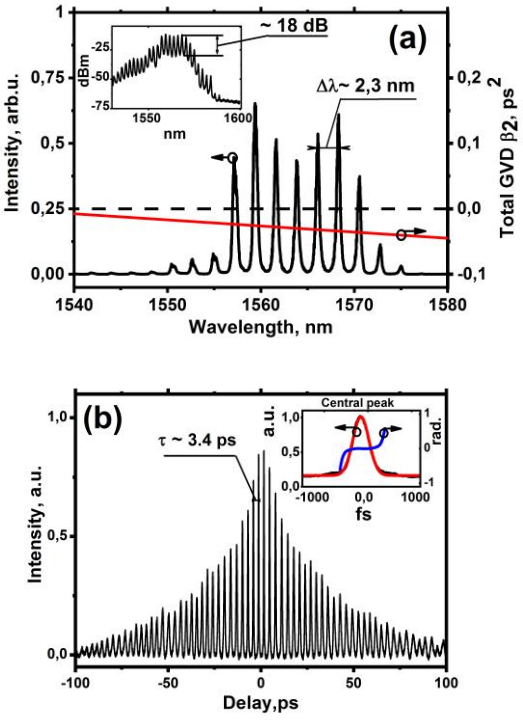

Fig. 4. (a) Pulse spectra and net-cavity GVD. Inset: pulse spectra on a dB scale. (b) Intensity autocorrelation trace. Inset: the central peak of the auto-correlation trace with Gaussian fitting and the pulse phase.

This article has been accepted for publication in a future issue of this journal, but has not been fully edited. Content may change prior to final publication. Citation information: DOI 10.1109/LPT.2019.2956570, IEEE Photonics Technology Letters

The output spectrum (see Fig. 4(a)) evidently shows high-contrast intensity fringes (~18 dB) that indicate a stable and strong coherent connection between the ultrashort pulses and fixed coherent phase difference in the temporal domain

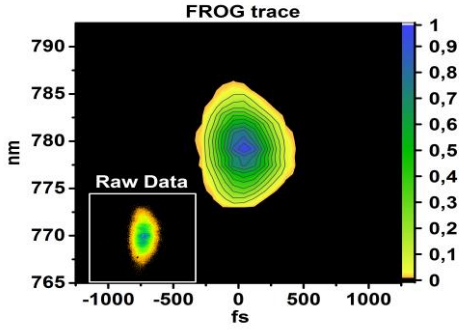

Fig. 5. SHG FROG trace of the MBS generation.

between several identical pulses [1]. The lack of symmetry could be attributed to the influence of high-order dispersion and the phase difference of π/2 between bound solitons [27]. The constant period of the sharp intensity fringes indicates the presence of several bound pulses with a stable time separation between them [15].

Fig. 4 (b) shows an intensity autocorrelation trace of the observed MBS generation (obtained by using the autocorrelator FR-103WS; FEMTOCHROME RESEARCH INC., Berkeley, CA, USA) and USP phase (by using Swamp Optics LLC, GRENOUILLE Model 15-40-USB, Georgia, USA) and the central autocorrelation peak with Gaussian fitting and the pulse phase (inset). More than 20 bound pulses are obtained with a constant intertemporal width of ~ 3.4 ps and a central peak duration of < 240 fs at full width at half maximum (FWHM) assuming Gaussian fitting which is ~19 pulse widths between pulses. The period of the spectral modulation (see Fig. 4(a)) is $\Delta\lambda$ = 2.3 nm ± 0.5 nm ($\Delta\nu$ = 281.3 GHz). The spectral modulation interfringe is inversely proportional to the temporal separation of the pulses $\tau = 1/\Delta\nu$. Thus, the calculated bound soliton separation τ = 3.6 ps ± 1.2 ps corresponds well to the experimental observation from the autocorrelation trace (3.4 ps). The Gaussian form of the autocorrelation central peak without a pedestal and the almost symmetrical form of the autocorrelation without additional intensity peaks along with the observed output spectra indicate that one pulse duration in the bond state is τ_{pulse} < 240 fs at FHWM with a stable temporal separation of pulses. Note that the asymmetrical form of the autocorrelation trace connected with the peak intensity can be attributed to the long averaging time of one trace exposure (100 times x 1 s ~ 1.5 min) and the significant noise floor of the autocorrelator.

Fig. 5 shows a second-harmonic generation (SHG) frequency-resolved optical gating (FROG) trace of the central autocorrelation peak, and the inset shows raw data from the matrix photodetector of the SHG FROG with a clear band structure. Moreover, we observed dechirped MBS generation according to the clean and symmetrical shape of the FROG trace and recalculated USP phase (inset of Fig. 4(b)). The calculated time-bandwidth product (TBP) for the spectral pulse width $\Delta\lambda_{FWHM}$ ~ 15 nm ($\Delta\nu_{FWHM}$ = 1.86 THz, see Fig. 4(a)) and the minimal pulse width τ_{min}~235 fs of the MBS is TBP = $\Delta\nu \times \tau_{min} \approx 0.446$ (the typical TBP value for Gaussian pulses is ≈ 0.441). Thus, the obtained MBS is close to its bandwidth-limit and dechirped character of the MBS generation is confirmed.

To characterize the short-term stability of the obtained MBS generation we measured the radio-frequency (RF) spectrum of the output pulse train and the relative intensity noise (RIN) of the developed laser at the maximal pump power of 500 mW. Fig. 6 shows a typical RF spectrum for the MBS regime at the fundamental oscillator frequency with a resolution of 300 Hz (using the ESA FSL 3 model.03; Rohde & Schwarz GmbH &

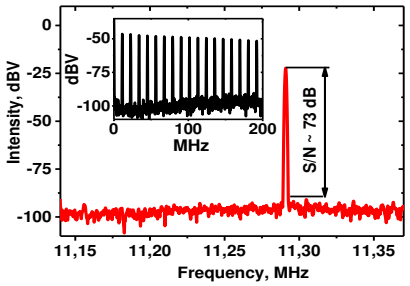

Fig. 6. RF spectrum of the pulse train at the repetition frequency. Inset: RF spectrum in the range 0-200 MHz.

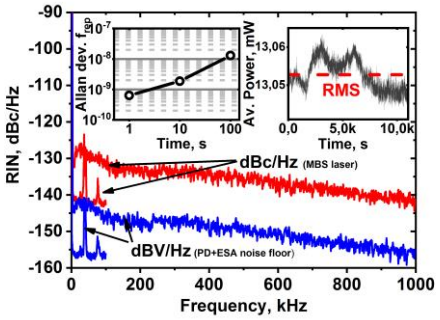

Fig. 7. RIN of the ML laser and noise floor from the PD+ESA. Inset: Allan deviation of the repetition rate and average output optical power during the measurement.

Co. KG, Munich, Germany). The RF spectrum has a peak at a frequency of ~11.3 MHz with a signal-to-noise (SNR) ratio of ~73 dB, and the absence of sidebands indicates the pulse-to-pulse MBS energy stability. The inset of Fig. 6 shows the RF spectrum in the frequency range of 30 kHz–200 MHz (resolution bandwidth of 3 kHz). The high SNR at the fundamental frequency and the absence of Q-switched sidebands in the RF spectrum prove the pulse-to-pulse stability of the ML regime.

Fig. 7 shows the RIN of the MBS laser (in [dBc/Hz]) at the maximal pump power of 500 mW and the noise floor from the photodetector (PD) and the electrical spectrum analyzer (in [dBV/Hz]) over a frequency range of 30 Hz – 1000 kHz (using ESA SR770FFT, Stanford Research Systems, California, USA over the frequency range from 30 Hz – 100 kHz and the Rohde & Schwarz ESA, above 100 kHz). For the MBS pulses at frequencies of ~30 Hz – 100 kHz, the RIN value was below -140 dBc/Hz, while at frequencies up to 1000 kHz, the RIN

value was below -125 dBc/Hz. Thus, we obtained an RIN value for the MBS laser that is comparable to that obtained previously by femtosecond combs based on other ML principles and USP generation regimes [28].

The long-term stability of the MBS generation can be characterized by the Allan deviation of the repetition rate (see the inset of Fig. 7 with 5 Hz data using Universal Counter 53132A, Agilent Inc., Santa Clara, CA, USA) for the free-running MBS fiber laser. The developed MBS laser has a relatively low repetition rate deviation with the value of $6.2 \cdot 10^{-10}$ for a 1 s interval, which is near the limit of the quartz oscillator frequency uncertainty and is determined only by the temperature drift during the averaging time interval of $1 - 1 \cdot 10^2$ s. It should be noted that we did not observe any pulse breaking or operation instabilities of the MBS generation during the experiment that lasted several hours. The inset of Fig. 7 demonstrates the average optical output power stability with a standard deviation of ~ 0.03 % RMS over a time of 10^4 s (measured by PM200 power meter with InGaAs detector S145C, Thorlabs Inc., Newton, New Jersey, US).

We obtained lower noise in the MBS operation at a high pump power than the previously observed high-energy ultrashort stretch-pulse generation in the same NPE-based ML fiber laser [25]. This fact is in good agreement with the theoretical analysis of the soliton energy quantization effect in a soliton fiber ring laser passively mode-locked by the NPE effect in Ref. [29]. The highest energy of a fundamental soliton with duration τ_p is limited by the soliton area theorem $Es \sim |\beta_2|/(\gamma \cdot \tau_p)$, where γ is the net nonlinear coefficient and β_2 is the total cavity dispersion. Soliton energy quantization results in pulse splitting at operation powers higher than the fundamental limit. Moreover, the energy quantization effect has been recently experimentally demonstrated by the dispersive Fourier transform technique (or time-stretch technique) in an SESAM mode-locked MBS fiber laser [11] with good agreement with the present results. Thus, MBS generation with N ~ 26 bound states is a natural consequence of the gain competition between multiple solitons and high-energy ultrashort stretch-pulse generation occurs in an NPE-based all-fiber erbium-doped ring laser with highly nonlinear resonator.

IV. Conclusions

In conclusion, low-noise multibound soliton generation is obtained (more than 20 bound pulses with an intertemporal width of ~ 3.4 ps) with an duration of ~ 240 fs at the repetition frequency of ~ 11.3 MHz (with a signal-to-noise ratio of ~ 73.3 dB) in the telecommunication spectral window in an erbium-doped all-fiber ring laser with a highly-nonlinear resonator mode locked by an NPE effect. Note that the relative intensity noise is <-140 dBc/Hz, and the Allan deviation of the repetition frequency does not exceed $\sim 1.3 \cdot 10^{-8}$ with a time averaging window of ~ 100 s.

References

[1] Chernysheva, M. *et al.*, "Double-Wall Carbon Nanotube Hybrid Mode-Locker in Tm doped Fibre Laser: A Novel Mechanism for Robust Bound-State Solitons Generation," *Sci. Rep.*, vol. 7, p. 44314, March 2017.

[2] Nhan Duc Nguyen, Le Nguyen Binh, "Generation of high order multi-bound solitons and propagation in optical fibers," *Optics Communications*, vol. 282, no. 12, pp. 2394-2406, 2009.

[3] A. Haboucha *et. al.,* "Analysis of soliton pattern formation in passively mode-locked fiber lasers," *Phys. Rev. A.*, vol. 78, p. 043806, 2008.

[4] Zajnulina *et. al.,* "Characteristics and stability of soliton crystals in optical fibres for the purpose of optical frequency comb generation," *Optics Communications*, vol. 393, pp. 95-102, 2017.

[5] Le Nguyen Binh, *Optical Multi-Bound Solitons. Optics and Photonics*., Taylor & Francis, 2015.

[6] Can Kerse *et al.,* "Ablation-cooled material removal with ultrafast bursts of pulses," *Nature*, vol. 537, pp. 84–88, 2016.

[7] Tong Zhou et al., "Coherent pulse stacking amplification using low-finesse Gires-Tournois interferometers," Opt. Express, vol. 23, pp. 7442-7462, 2015.

[8] Boris A. Malomed, "Bound solitons in coupled nonlinear Schrödinger equations," *Phys. Rev. A*, vol. 45, p. R8321, 1992.

[9] C. Luo, S. Wang, and Y. Lai, "10 GHz Bound Soliton Mode-locking in an Environmentally Stable FM Mode-locked Er-doped Fiber Soliton Laser," in *CLEO: 2014, OSA Technical Digest (online) (Optical Society of America, 2014)*, p. JTu4A.69, 2014.

[10] Weiqiang Wang *et al.,* "Robust soliton crystals in a thermally controlled microresonator," *Opt. Lett.,* vol. 43, pp. 2002-2005, 2018.

[11] Shuqian Sun *et al.*, "Time-stretch probing of ultra-fast soliton dynamics related to Q-switched instabilities in mode-locked fiber laser," *Opt. Express*, vol. 26, pp. 20888-20901, 2018.

[12] Y. F. Song *et al.*, "Coexistence and interaction of vector and bound vector solitons in a dispersion-managed fiber laser mode locked by graphene," *Opt. Express*, vol. 24, pp. 1814-1822, 2016.

[13] Yadong Wang *et al.*, "Harmonic mode locking of bound-state solitons fiber laser based on MoS_2 saturable absorber," *Opt. Express*, vol. 23, pp. 205-210, 2015.

[14] Zhenhong Wang *et al.,* "Generation of harmonic mode-locking of bound solitons in the ultrafast fiber laser with Sb_2Te_3 saturable absorber on microfiber," *Laser Physics Letters*, vol. 16, p. 025103, 2019.

[15] Ph. Grelu *et al.*, "Phase-locked soliton pairs in a stretched-pulse fiber laser," *Opt. Lett.*, vol. 27, pp. 966-968, 2002.

[16] L. M. Zhao *et al.*, "Bound states of dispersion-managed solitons in a fiber laser at near zero dispersion," *Appl. Opt.*, vol. 46, pp. 4768-4773, 2007.

[17] A. Komarov *et al.*, "Multistability and hysteresis phenomena in passively mode-locked fiber lasers," *Phys. Rev. A*, vol. 71, p. 053809, 2005.

[18] Adil Haboucha *et al.*, "Coherent soliton pattern formation in a fiber laser," *Opt. Lett.,* vol .33, pp. 524-526, 2008.

[19] Foued Amrani *et al.*,"Universal soliton pattern formations in passively mode-locked fiber lasers," *Opt. Lett.,* vol. 36,pp. 1545-1547, 2011.

[20] Jérôme Lhermite *et al.*,"Tunable high-repetition-rate fiber laser for the generation of pulse trains and packets," *Opt. Lett.,* vol. 32, p. 1734, 2007.

[21] A. Andrianov and A. Kim, "Extremely elastic soliton crystals generated in a passively mode-locked tunable high-repetition-rate fiber laser," *arXiv [physics.optics]*, 1905.03129v1, 2019.

[22] D. A. Dvoretskiy *et al.*, "Ultrashort Multi-Bound Solitons Generation in the Passively Mode-Locked All-Fiber Laser at the Telecom Window," *2018 European Conference on Optical Communication (ECOC)*, Rome, 2018, pp. 1-3.

[23] Y. Yatsenko and A. Mavritsky, "D-scan measurement of nonlinear refractive index in fibers heavily doped with GeO2," *Opt. Lett.*, vol. 32, pp. 3257–3259, 2007.

[24] A.E. Levchenko, *et al.*, "Measurement of dispersion in optical fibres with a microstructure cladding," *Quantum Electronics*, vol. 35, no 9, pp. 835-838, 2005.

[25] Dmitriy A. Dvoretskiy *et al.*, "High-energy ultrashort-pulse all-fiber erbium-doped ring laser with improved free-running performance," *J. Opt. Soc. Am. B*, vol. 35, pp. 2010-2014, 2018.

[26] Dmitriy A. Dvoretskiy *et al.*, "Multibound solitons generation with a controllable number of bound states in a passive mode-locked all-fiber erbium-doped ring laser," *Proc. SPIE,* vol. 11026, p. 110260Q, 2019.

[27] Lili Gui *et al.*, "Soliton Molecules and Multisoliton States in Ultrafast Fibre Lasers: Intrinsic Complexes in Dissipative Systems," *Applied Sciences*, vol. 8, no. 2, p. 201, 2018.

[28] Jungwon Kim and Youjian Song, "Ultralow-noise mode-locked fiber lasers and frequency combs: principles, status, and applications," *Adv. Opt. Photon.,* vol. 8, pp. 465-540, 2016.

[29] D. Y. Tang, L. M. Zhao, B. Zhao, and A. Q. Liu "Mechanism of multisoliton formation and soliton energy quantization in passively mode-locked fiber lasers," *Phys. Rev. A*, vol. 72, p. 043816, 2005.